Improving the efficiency of electrochemical CO_2 reduction using immobilized manganese complexes

James J. Walsh‡, Charlotte L. Smith‡, Gaia Neri, George F. S. Whitehead, Craig M. Robertson and Alexander J. Cowan*

Department of Chemistry, Stephenson Institute for Renewable Energy, The University of Liverpool, L69 7ZF, Liverpool, UK.

E-mail: a.j.cowan@liverpool.ac.uk. ‡These authors share equal contribution.

Electronic supplementary information

Contents:

1. Experimental

*1.1 Synthesis of **1** and **2***

[Mn(bpy)$(CO)_3$Br] (**1**)

Yield = 80.04 %; ^{1}H-NMR (CD_3CN, 400 MHz): δ = 9.22 (d, *J* = 5.5 Hz, 2 H), 8.34 (d, *J* = 8.0 Hz, 2 H), 8.12 (t, *J* = 1.0 Hz, 2 H), 7.61 ppm (t, *J* = 6.5 Hz, 2 H); ^{13}C-NMR (CD_3CN, 101 MHz): δ = 156.6, 154.5, 140.1, 140.0, 136.2, 129.7, 127.6, 127.5, 124.0, 118.3 ppm; FTIR (CH_3CN): 2027, 1934, 1922 cm^{-1}; Anal. calcd. for $C_{13}H_8BrMnN_2O_3$: C, 41.64; H, 2.15; N, 7.46. Found: C, 41.59; H, 2.06; N, 7.34. m/z (ESI); 327 ($[M\text{-}Br^- + HOMe]^+$), 295 ($[M\text{-}Br^-]^+$).

[Mn(bpy(^{t}Bu)$_2$)$(CO)_3$Br] (**2**)

Yield = 42.51 %; ^{1}H-NMR (CD_3CN, 400 MHz): δ = 9.08 (d, *J* = 5.9 Hz, 2 H), 8.35 (d, *J* = 1.4 Hz, 2 H), 7.62 (dd, *J* = 5.8, 1.7 Hz, 2 H), 1.45 ppm (s, 18 H); ^{13}C NMR (CD_3CN,101 MHz): δ = 164.2, 156.1, 153.7, 124.3, 120.9, 117.9, 35.8, 30.0 ppm; FTIR (CH_3CN): 2024, 1947, 1914 cm^{-1} ; Anal. Calcd. for $C_{21}H_{24}BrMnN_2O_3$: C, 51.75; H, 4.94; N, 5.76. Found: C, 51.74; H, 4.89; N, 5.59. m/z (ESI); 439.1 ($[M\text{-}Br^- + HOMe]^+$), 407 ($[M\text{-}Br^-]^+$).

1.2 X-ray crystallography

Data for structures **3** and **4** were collected on a Rigaku MicroMax™-007 HF with a molybdenum rotating anode microfocus source and a Saturn 724+ detector. Full crystallographic details for all crystal structures are included in Table S1. CCDC 1061484-1061485 contain the supplementary crystallographic data for this paper. These data can be obtained free of charge from The Cambridge Crystallographic Data Centre via www.ccdc.cam.ac.uk/data_request/cif.

X-ray quality crystals were grown by slow vapour diffusion of *n*-hexane into concentrated THF or acetone solutions of complex to afford block crystals of **3** and **4**, respectively.

Complex **3** crystallized in the P21/c space group containing 4 independent molecules per unit cell. There were two THF molecules and one water of crystallization. The (bpy$(COOH)_2$) ligand in **3** is more distorted out of plane than in **4** with Br-Mn-N bond angles of 88.81º and 85.55º, reducing the symmetry of the system somewhat. There was disorder in the crystals, leading to 7 % occupancy for bromide in the axial carbonyl site. This is not *fac-mer* isomerization, which has been seen previously in the solid state for Mn bipyridyl complexes, but rather partially disordered crystal growth induced by the bipyridyl ligand asymmetry and complex inversion.[S1]

Complex **4**, as the *fac* isomer only, crystallized in the P-1 space group containing 2 independent molecules per unit cell. The Mn-Br bond length was 2.56 Å, compared with 2.51 Å in **2**. The Br-Mn-N bond angles are 86.68º and 86.06º, indicating slight out-of-plane ligand distortion.

Table S1: Crystallographic Details

Compound	**3**	**4**
Formula	C_{23} $H_{26}BrMnN_2O_{10}$	$C_{13}H_8BrMnN_2O_5$
M_r	621.31	407.06
Crystal System	triclinic	monoclinic
Space Group	P-1	$P2_1/c$
a [Å]	6.52291 (18)	15.1341 (2)
b [Å]	13.864 (4)	13.1528 (2)
c [Å]	16.0537 (4)	7.05370 (10)
α [°]	102.912 (3)	90
β [°]	95.846 (2)	98.591 (2)
γ [°]	98.907 (2)	90
V [Å^3]	1317.58 (7)	1388.33 (3)
Z	2	4
ρ_{calcd} [mg mm^{-3}]	1.576	1.948
T [K]	100	100
Shape and color	Block, Orange	Block, Orange
Size (mm)	0.3 × 0.2 × 0.2	0.2 × 0.2 × 0.2
λ / Å	0.71073	0.71073
μ / mm^{-1}	2.074	3.854
Unique data	5384	4417
Absorption correction	multi-scan	multi-scan
transmission max/min	1.00000/0.88776	1.0000/0.75509
unique data [F_o > **4**F_o)]	4404	3815
parameters/restraints	363/2	201/0
Goof on F^2	1.028	1.047
R_1 [I>2σ (I)]	0.0396	0.0359
wR_2 [all data]	0.0863	0.0962
weighting scheme[b] [w^{-1}]	1/[σ^2(F_o^2) + (0.0364P)^2 + 0.9585P]*	1/[σ^2(F_o^2) + (0.0504P)^2 + 1.3888P]*
largest residuals [e Å^{-3}]	0.513, −0.338	0.700, -0.990

* where P = 1/3[max(F_o^2,0) + 2F_c^2]

1.3 ORTEP diagrams

ORTEP diagrams are given at 50 % probability.

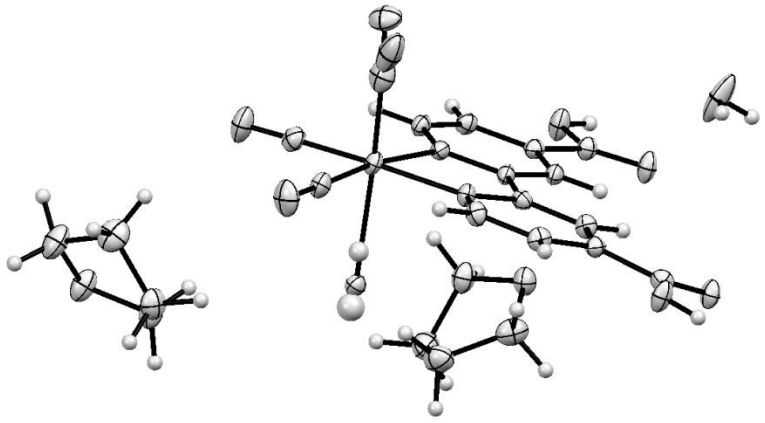

Fig. S1: ORTEP diagram of complex **3**. The unit cell includes two THFs and one water of crystallization. The axial bromide is disordered, with 7 % occupancy in the opposite (carbonyl) ligand position.

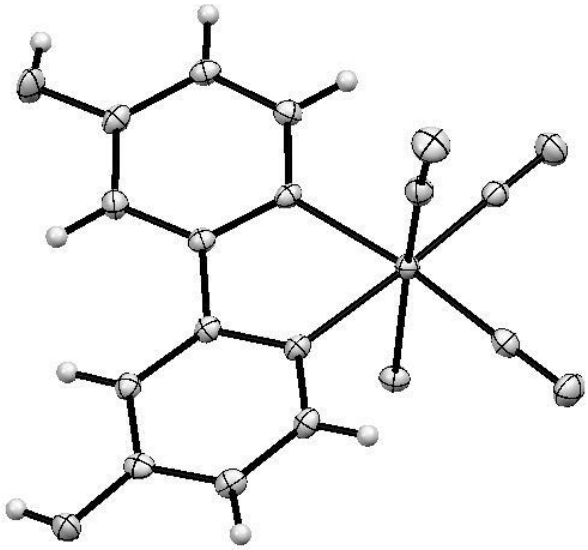

Fig. S2: ORTEP diagram of complex **4**.

2. Spectroscopy and electrochemistry

*2.1 FTIR spectroscopy of **2**-**4** in solution*

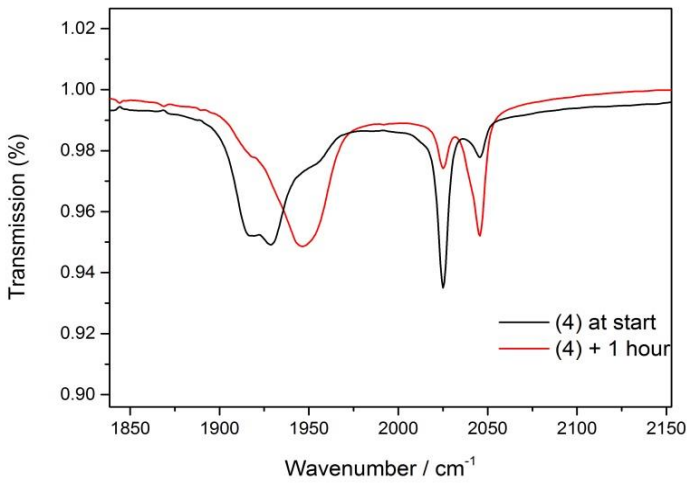

Fig. S3: FTIR spectra of **4** in dry CH_3CN *ca*. 5 minutes after dissolution (black) and 1 hour after dissolution (red), showing the conversion of $[Mn(bpy(OH)_2)(CO)_3Br]$ to $[Mn(bpy(OH)_2)(CO)_3(Solv)]^+$.

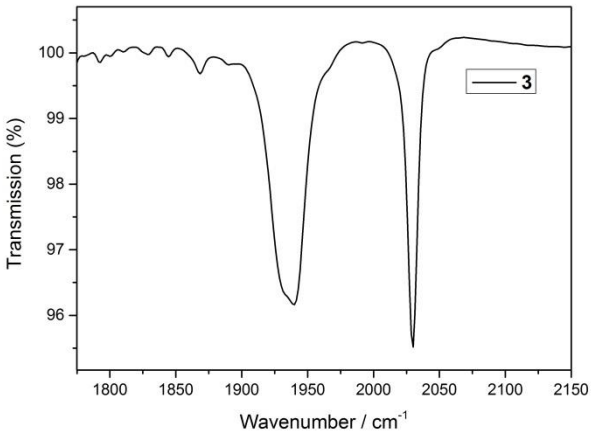

Fig. S4: FTIR spectra of **3** in CH_3CN *ca*. 5 minutes after dissolution. No observable ligand exchange occurs on the timescale of minutes.

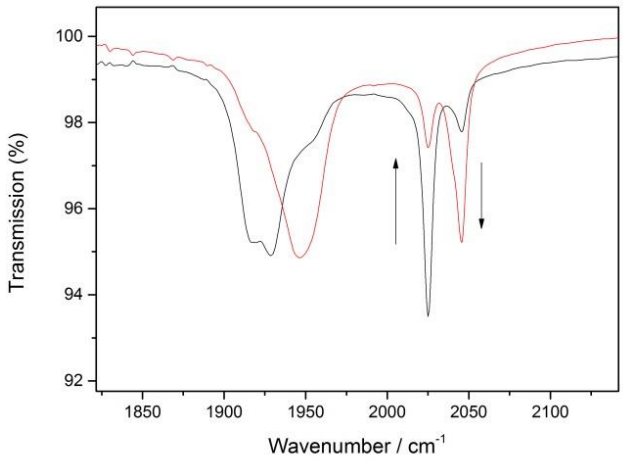

Fig. S5: FTIR spectra of **2** in dry CH_3CN 60 minutes (black) and 24 hours (red) after dissolution showing the conversion of $[Mn(bpy(^tBu)_2)(CO)_3Br]$ to $[Mn(bpy(^tBu)_2)(CO)_3(Solv)]^+$.

*2.2 Solution phase CVs of complexes **1**-**4***

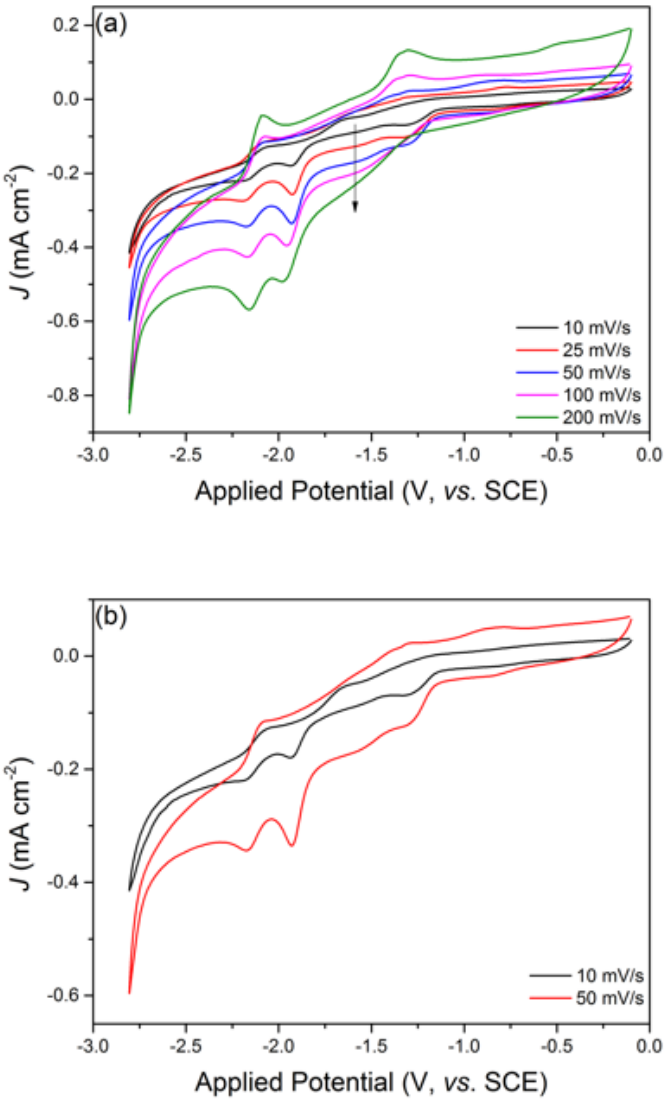

Fig. S6: CVs of complex **4** in dry MeCN/0.1 M TBA PF_6. Glassy carbon working electrode (A = 0.0717 cm^2), Pt counter, Ag wire pseudo-reference calibrated *vs.* the Fc/Fc^+ redox couple. (a) Scan rates from 10 mV/s to 200 mV/s, showing the evolution of peak II. (b) Scan rates at 10 and 50 mV/s highlight peak II further.

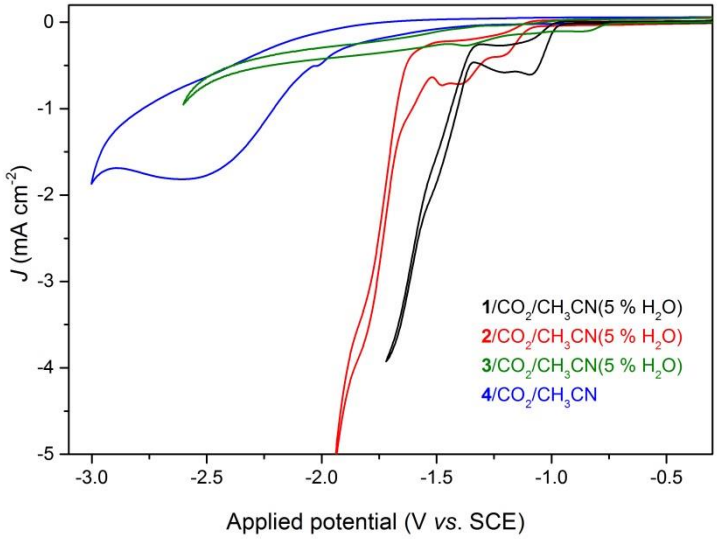

Fig. S7: Cyclic voltammetry comparing activity of all catalysts. Complexes **1**, **2** and **3** were studied in CH_3CN/H_2O (95:5) and complex **4** in dry CH_3CN. Scan rates were 100 mV/s, supporting electrolyte was 0.1 M TBA PF_6, glassy carbon working electrode, Pt counter electrode, CO_2-purged.

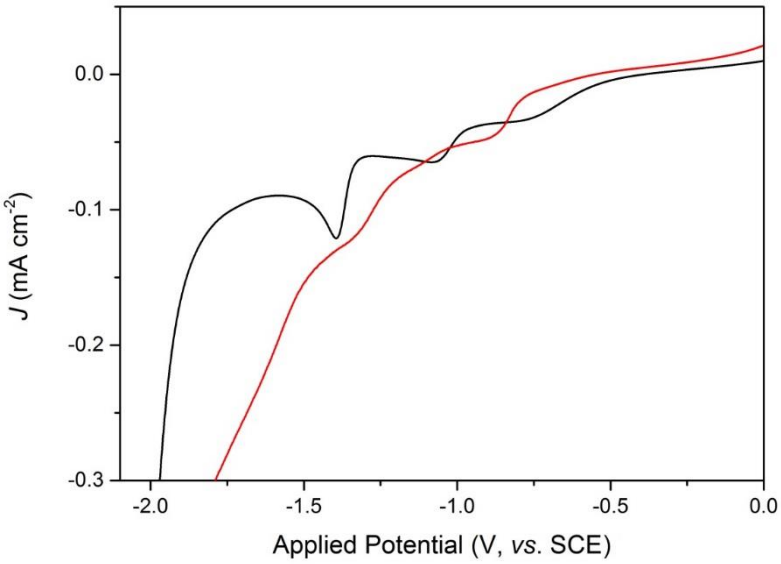

Fig. S8: Linear sweep voltammograms of **3** in $MeCN/H_2O$ (95:5) containing 0.1 M TBA PF_6 under Argon (black) and CO_2 (red) at 10 mV/s. Sweeps were run in the cathodic direction.

2.3 IR-SEC curve fitting

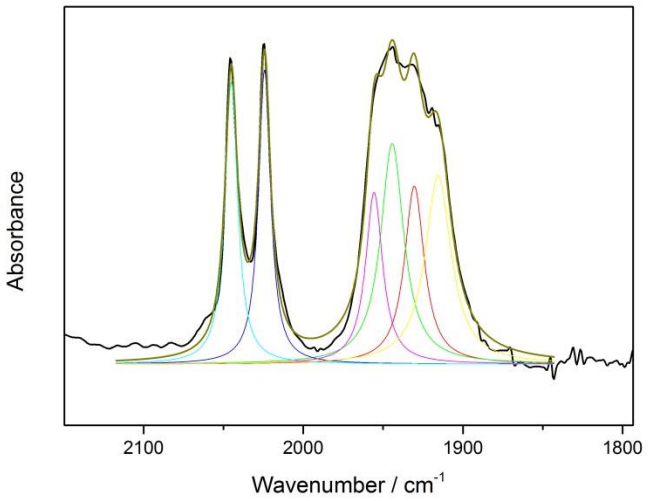

Fig. S9: Multi-Lorentzian fit of FTIR spectra of **4** in dry CH_3CN *ca*. 30 minutes after dissolution showing multiple overlapping contributions from the presence of [Mn(bpy(OH)$_2$)(CO)$_3$Br] (2024, 1930 and 1915 cm^{-1}) and [Mn(bpy(OH)$_2$)(CO)$_3$(CH_3CN)] (2044, 1955 and 1944 cm^{-1}).

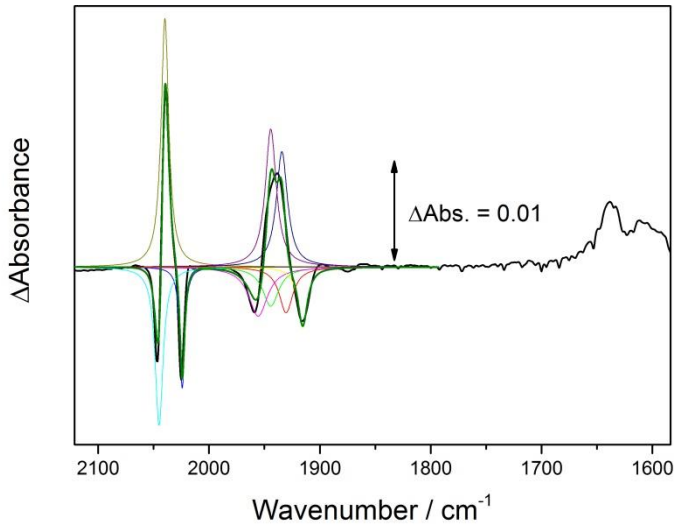

Fig. S10: Multi-Lorentzian fit of FTIR difference spectra of **4** upon initial reduction in CH_3CN. The spectrum obtained is shown as the difference versus that measured at open circuit. Negative bands indicate the loss of the starting material, positive the growth of a new species. The frequencies and widths of the ν(CO) bands of **4** and its solvent complex were fixed at the values obtained in Fig. S9 during fitting and a new tricarbonyl species is apparent, which is assigned to [Mn(bpy(OH)(O^-))(CO)$_3$(Solv)].

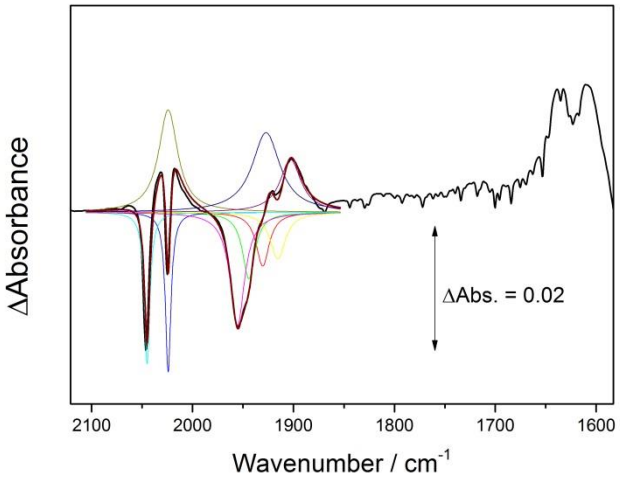

Fig. S11: Multi-Lorentzian fit of FTIR difference spectra of **4** in CH_3CN reduced during process III. The spectrum is the difference versus that measured at open circuit. Negative bands indicate the loss of the starting material, positive the growth of a new species. The frequencies and widths of the ν(CO) bands of **4** and its solvent complex were fixed at the values obtained in Fig. S9 during fitting.

3 Thin film electrochemistry

*3.1 Solution vs. immobilized CVs of **2***

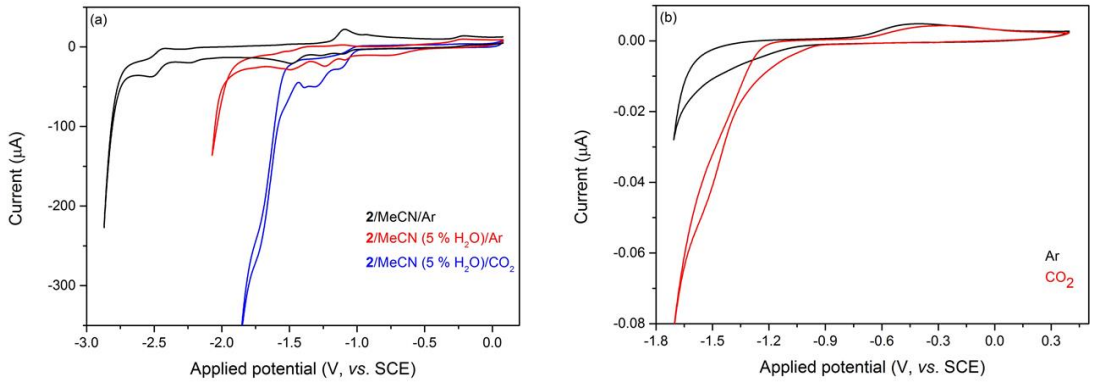

Fig S12: CVs of **2** in solution (a) and immobilized in a Nafion/MWCNT film (b). Potentials have been corrected to *vs*. SCE.[S2]

*3.2 Role of CO_2 re-purges on CPE of **2**/MWCNT/Nafion cathodes*

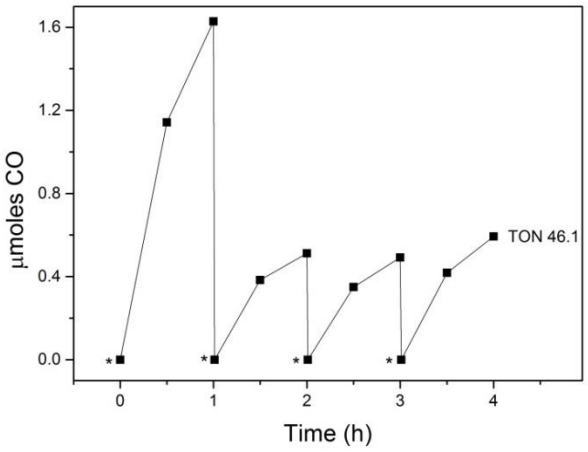

Fig. S13: Gas product evolution during CPE of **2/**MWCNT/Nafion at -1.5 V in .1 M phosphate buffer (pH 7) under CO_2, After each hour the experiment was paused and re-purged with CO_2 for 20 minutes (marked with *). The experiment was restarted and an injection taken to confirm evacuation of CO and H_2 from previous cycle.

3.3 Temperature dependence of drop drying on film CVs

The effects of temperature on drop drying were investigated by holding the temperature constant in a small dark room using the thermostat and leaving the drop-cast film to dry overnight. CVs of the films under identical conditions (*vs*. Ag/AgCl, Pt counter, 0.05 M NaH_2PO_4 + 0.05 M Na_2HPO_4 electrolyte, 100 mV/s scan rate) showed significant differences with those recorded at the higher temperatures, >23 ^oC giving far higher current densities under argon. The higher current density under argon for the reverse dimer oxidation, centred at ~ -0.2 V in Fig. S14 indicates that a far higher concentration of the originally deposited material is able to undergo electrochemical reduction and subsequent dimerization.

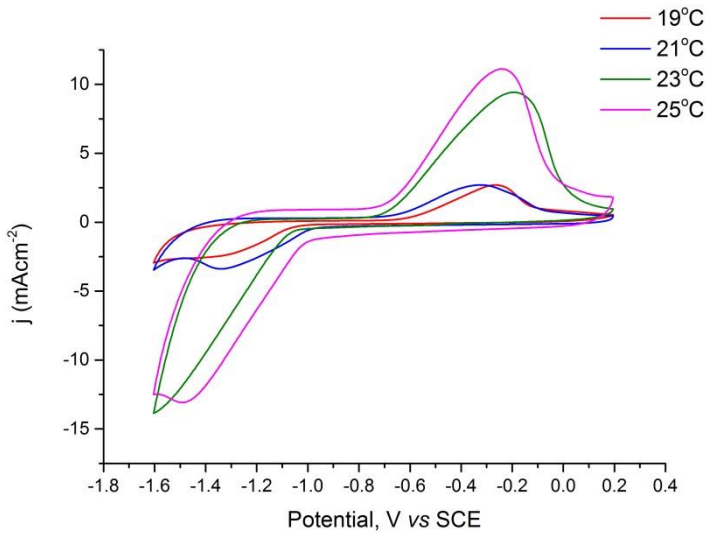

Fig. S14: CVs of films of **1** dried at different temperatures. *v* = 100 mV.s^{-1}.

3.4 Percentage electroactive calculations

The number of moles of electroactive material that are able to dimerise can be calculated using Equation S1 and slow scan rate (10 mV.s^{-1}) CV data:

$$\Gamma = \frac{Q}{nFA} \quad \text{(S1)}$$

Where Γ is the electroactive surface coverage (moles.cm^{-2}), Q is the charge passed (C), n is the formal number of electrons transferred, F is Faraday's constant (96485 C.mol^{-1}) and A is the geometric surface area of the glassy carbon working electrode (0.0717 cm^2). Based on these calculations the % of Mn electroactive at each temperature is increased from *ca*. 8 % at 19^{o}C to 27 % at 25^{o}C.

3.5 Temperature dependence of drop drying on film morphologies

We also examined the effect of drying temperature on the film morphology. Profilometry studies were carried out on samples dried on glass slides under identical conditions to those used for casting onto a glass carbon electrode. At all temperatures, clustering of material was found to occur and the electrode surface was extremely rough, Fig. S15. Interestingly the films dried at higher temperatures appeared to contain a high number of very large clustered features.

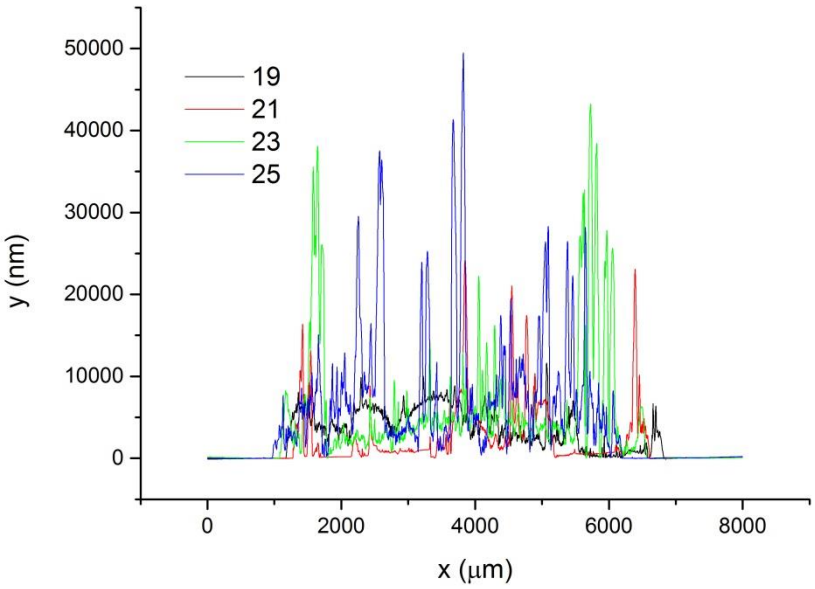

Fig. S15: Profilometry of drops cast under temperature control onto glass slides. Drying temperatures in degrees C.

References

S1: A. J. Blake, N. R. Champness, T. L. Easun, D. R. Allan, H. Nowell and M. W. George, *Nature Chem*., 2010, **2**, 688-694.

S2: V. V. Pavlishchuk and A. W. Addison, *Inorg. Chim. Acta*, 2000, **298**, 97-102.